COMPARISON OF ASPECT RATIO, ACCURACY AND REPEATABILITY OF A LASER LINE SCANNING PROBE AND A TACTILE PROBE

Bart BOECKMANS[1], Min ZHANG[1,2], Frank WELKENHUYZEN[1] , Wim DEWULF[3] and Jean-Pierre KRUTH[1]

1 KU Leuven, Dep. Mechanical Engineering, Div. PMA, Celestijnenlaan 300B, B-3001 Leuven, Belgium, Bart.Boeckmans@kuleuven.be
2 College of Mech. Eng. and Applied Electronics Tech., Beijing University of Technology, Beijing 100124, China
3 KU Leuven, Campus Groep T, A. Vesaliusstraat 13, B-3000 Leuven, Belgium

Abstract:
Laser line scanning is a laser based measurement method to acquire dimensional information of a workpiece. The most common applications are found in e.g. automotive and medical industry. The advantages of laser line CMM probing are a high data density and a high measurement speed. This makes the probe ideal to measure three dimensional free form surfaces. To align freeform parts in a precise manner however, features (e.g. cylinders, spheres) are used to allocate the position. The newest generation of laser line scanners can have an MPE_P of below 10µm.

The first part of the paper presents a reference object with drilled holes of different diameters. The influences of the diameter of the feature and the in-plane viewing angle on the measuring depth range are investigated on this reference object. The results can then be converted to an aspect ratio limitation that restricts the feature dimensions for full inspection. The second part compares the accuracy and the repeatability of a Nikon Metrology LC60Dx digital laser line scanner and a Renishaw TP200 touch-trigger probe, using two case study objects that incorporate cylindrical features. The experimental case takes into account different surface finishes and the previously acquired results on the aspect ratio of the measurement. Both investigated sensors are equipped on the same CMM and are operated with the same software**.**

Keywords: Dimensional metrology, CMM, Laser Scanning, Accuracy, Repeatability.

1. INTRODUCTION

A laser line scanner is a sensor type which can be used as a replacement for or a contributor to a tactile probe on a coordinate measuring machine (CMM). Combining the laser scanner with a tactile probe gives the possibility to improve the large datasets of the laser scanner by offsetting it based on more accurate tactile measurements [1]. The non-contact technique of laser line scanning is based on the triangulation principle depicted in Fig. 1a and thoroughly described in [2]. The opening angle γ between the laser plane and viewing plane shown in Fig. 1a is a parameter which is fixed by the scanner construction. Since the region where the projected laser plane and the view of the digital camera meet is finite, the scanner as a system has a field of view (FOV) limitation (Fig. 1b) [2, 3]. Advantages and disadvantages compared to tactile probing have been discussed in depth [3, 4, 5]. Advantages consist of contact free measurement without measuring forces, high data density and high measurement speed (e.g. 75.000 points/sec). Disadvantages are the influences of the part properties and the measurement settings. The parts finishing parameters (e.g. translucency, surface colour, roughness and reflectivity [1, 6]) influence the measurement with a laser scanner, where tactile probing is influenced mainly (but less) by surface roughness. The larger variety in settings (e.g. laser intensity, exposure time, filter settings, sensor in-plane and out-of-plane angle) are prone to raise the operator influence and hence lower the reproducibility of the measurement. Next to the accuracy, the repeatability obtained with a fixed measurement setting is a focus of this paper.

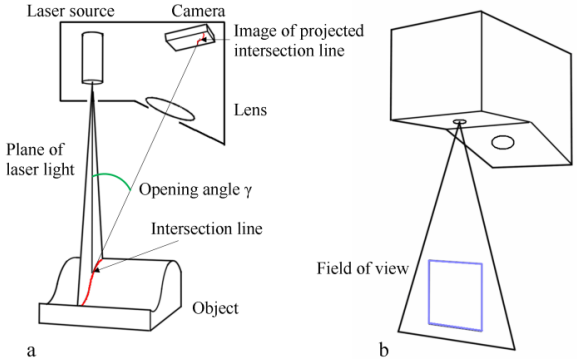

Fig. 1: a) Laser triangulation principle; b) field of view (FOV) restriction [2].

The accuracy of laser scanners improved tremendously over the last decade. There has been progress in identifying the measurement accuracy for optical sensors like laser line scanners [7, 8, 9]. Today a standard exists [10] and accuracy tests have been introduced to test the accuracy and repeatability [2, 11, 12].

This paper first discusses the materials and methods used in testing hole measurements with a laser scanning probe (section 2). Section 3 scrutinises the influence of the hole dimensions and the measurement sensor orientation on the maximum measurement depth and the measurement accuracy. The findings of the influence are then tested in a case study using two identical parts but with different surface finish (section 4). The last section embodies the conclusions of the research.

2. MATERIALS AND METHODS

2.1 Measurement equipment

All measurements mentioned in this paper made use of an LK Altera CMM (Fig. 2a). The CMM has the following uncertainty specification, dependent on the measurement length L (in mm) and expressed in µm.

$$MPE_P = 1.8 + L/400 \quad (1)$$

Through an indexable Renishaw PH10M rotary head the machine can be equipped with a variety of probes. The probes used in this study comprise of a Renishaw TP200 touch-trigger probe (Fig. 2b) and a Nikon Metrology LC60Dx laser scanner (Fig. 2c). The TP200 connection is equipped with a 20mm long stylus with a diameter of 1mm and has an MPE_P value of 1.7µm. The LC60Dx has an MPE_P value of 9µm (in accordance with ISO 10360-1 [13] and ISO 10360-8.2 [10]).

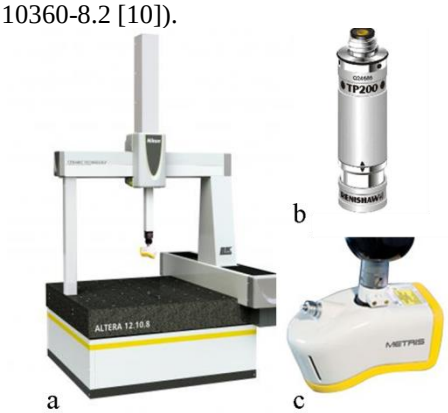

Fig. 2: Measurement equipment: a) LK Altera 12.10.8 CMM; b) Renishaw TP200 touch-trigger probe; c) Nikon Metrology LC60Dx laser scanner.

2.2 Reference artefact and case study object

The measurements make use of a testing artefact and two case study workpieces. The hole block artefact (Fig. 3a) has 6 ground surfaces and 12 drilled and reamed holes with decreasing diameter (20, 15, 10, 9, 8, …, 3, 2 and 1mm). All surfaces were ground and the top surface was reground after the holes were reamed to assure a minimum of burr formation and to exclude possible chamfering from deburring after drilling. The case study workpieces are industrial parts (Fig. 3b) with cylindrical cavities of different diameters (3mm - 8.5mm) that have different tolerance zones (0.06mm - 0.2mm). The focus of this paper goes to the 8.5mm holes which have a position tolerance zone of 0.2mm.

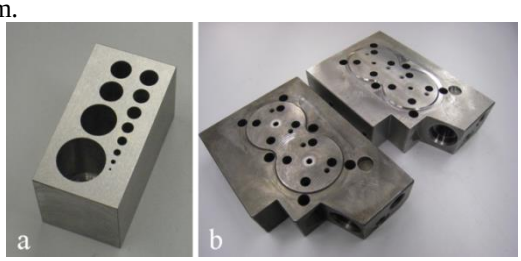

Fig. 3: Measurement objects: a) hole block reference object; b) industrial case study objects (matt and shiny).

2.3 Measurement method

In the case study incorporated in the paper (section 4) two measurement methods are used to determine the diameter and position of the cylindrical cavities in the case study objects. The first method makes use of the guidelines given by the manufacturer of the optical measurement sensor. The second method is determined in section 3.

The tactile measurements are conducted with a single sensor orientation, while the optical measurement requires the use of more sensor orientations. The different sensor orientations give the possibility to assess the part from different viewing angles. The multiple point clouds obtained are then merged and filtered before the feature extraction takes place.

In the experiment for the aspect ratio determination separate measurements are conducted for the investigation of the influence of the in-plane angle setting in combination with the size of the cavity (section 3). Five configurations for the in-plane angle α are used.

3. ASPECT RATIO TEST USING DRILLED HOLE REFERENCE OBJECT

3.1 Experiment

The aspect ratio test described below has two objectives. Firstly, the aspect ratio limitation of a cylindrical cavity for it to be assessed fully in an accurate and repeatable fashion is determined. To make a statement on the accuracy, a tactile reference measurement is executed. Both the maximum depth and the accuracy are expressed in function of the hole diameter and the in-plane angle α of the laser scanner. The in-plane angle is shown in Fig. 4 [2]. This angle is measured with respect to the z axis of the CMM. Secondly, conclusions are drawn about the presence of a preferable region to measure a drilled hole in terms of accuracy and stability. The artefact used for this test is described in section 2.2 and shown in Fig. 3a.

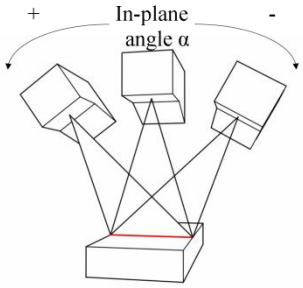

Fig. 4: The in-plane angle setting for a laser scanner [2].

The measurement follows the steps described next. First a calibration is performed for the tactile probe (1) to fix the probe compensation and measurement tool offset to the machine coordinate system (MCS). Subsequently a manual pre-alignment (2) and an automatic alignment (3) of the workpiece are conducted with the tactile probe. By first doing a basic pre-alignment (3-2-1 alignment method) the amount of manual handling is limited. The main automatic alignment is more accurate (RPS-based with more points) and ensures the operator influence to be minimized to the best possible extent. The following step consists of the tactile measurements (4). Then the sensor change to the laser scanner takes place and the laser scanner is calibrated (5). The choice to not calibrate the optical sensor at the start can be ascribed to the attempt to rule out changes in the tool offset after removing and replacing the sensor. Lastly the optical measurements are executed (6).

The measured cylindrical features have different diameters (20, 15, 10, 9, 8, ..., 2 and 1mm). All features are measured on different depths, going from 1mm inside the cavity down to the maximum possible, in steps of 0.5mm.

3.2 Results

3.2.1 Maximum depth in function of hole diameter and in-plane angle

Figure 5 shows the maximum depth obtained for each combination of hole diameter and in-plane angle. This maximum is determined as the lowest maximum of 5 measurements (excluding outliers). For instance for a hole diameter of 8mm and an in-plane scanner angle of 30 degrees, the maximum depth at which the scanner could extract a 2mm high cylindrical area from the point cloud and fit a cylinder in this point cloud is 14mm. The expected downward trend for decreasing diameter and increasing in-plane angle α are well visible. Measuring at an in-plane angle of 15° turns out to be less reliable, as is mentioned in the guidelines of the scanner. Most probably the chosen settings, namely the combination of the in-plane angle and the measurement path, result in an incomplete point cloud.

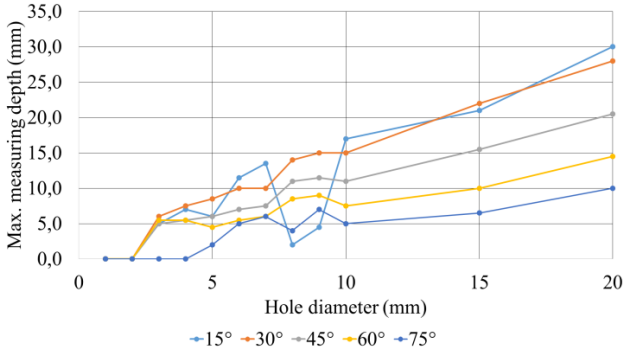

Fig. 5: Maximum measurement depth in function of the in-plane angle and the hole diameter.

3.2.2 Accuracy in function of measuring depth

The error results for the consecutive feature extractions from an optical point cloud for a hole of diameter 15mm are presented in Fig. 6 against the measuring depth. The error is calculated as the difference from the tactile reference measurement taking into account the full cylinder (i.e. tactile measurements over the total reachable height of the hole). In this case the average x positions, y positions and diameters (determined for a total of 5 measurements) are shown in function of the depth of the feature extraction of the diameter 15mm cylindrical cavity.

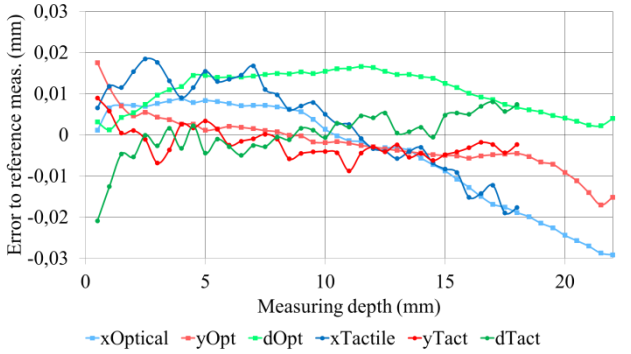

Fig. 6: Measurement results for the diameter 15mm hole from the aspect ratio test. Diameter, x and y position of both the optical and the tactile measurement are integrated.

The graph (Fig. 6) also displays the tactile measurement error results for varying measurement depth. It shows that the errors on x and y position resemble for the tactile and laser sensor, but differ somewhat for the hole diameter, yet having the same order of magnitude.

3.3 Discussion

3.3.1 Maximum depth in function of hole diameter and in-plane angle

The possible scanning depth can be derived theoretically with the following formulas. First of all the laser depth t_1, relates to a tangent equation (Eq. 2), where c_1 is the chord length of the intersection of the projected laser plane with the virtual top plane of the hole and α is the in-plane angle (Fig. 4).

$$c_1 = t_1 \cdot \tan\alpha \qquad (2)$$

The maximum laser depth $t_{1,max}$ is the optimum of this function, where the chord length c_1 reaches its maximum, being the diameter d. This maximum is reached for the laser plane in Fig. 7a. In all parts of Fig. 7 the red plane is the laser line projection plane and the green plane is the midplane of the field of view (FOV) of the recording camera sensor. The coloured intersection lines with the cylinder mantle and the virtual top surface of the cavity are also shown. The latter shows the magnitude of the chord length within this circular top plane.

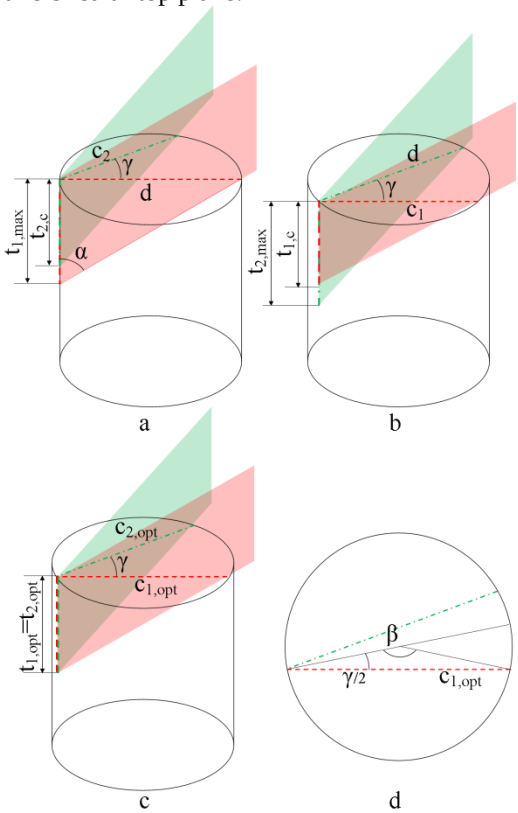

Fig. 7: Situational sketches: a) maximum laser depth $t_{1,max}$; b) maximum viewing depth $t_{2,max}$; c) optimum combination $t_{1,opt}$ and $t_{2,opt}$; d) top view for optimal chord length (c_{opt}) determination.

The laser depth however is only a part of the sensors needs. The projected laser line has to be seen by the CMOS camera as well. Therefore the opening angle γ of the scanner

(Fig. 1a) has to be taken into account, which in this case is 30 degrees. The camera depth t_2 is determined in an analogue manner, and has the same value for maximum depth as the laser depth ($t_{1,max}$ equals $t_{2,max}$). Figure 7a and 7b however show that these maxima do not occur at the same time during the scanning movement. When one of the two (laser or viewing) is at its maximum, the other only uses a limited chord length. The optimum is depicted in Fig. 7c. In this case both the laser and the camera depth use the same chord length c_{opt}. This chord length can be determined by Eq. 3, with dependence on the diameter and the inscribed angle β (Fig. 7d).

$$c = d \cdot \sin\frac{\beta}{2} \qquad (3)$$

The inscribed angle is dependent on the angle between the projected laser plane and the viewing direction, through geometrical definitions. In worst case the angle between the laser plane and viewing plane would go up to the opening angle γ of the scanner. Figure 7d shows the bisector in this ideal location, which is part of the isosceles triangle together with one of the two top plane intersection lines. The inscribed angle in the circle centre has a worst case value β equal to 150°. Combining Eq. 2 and Eq. 3 to evaluate the optimum laser depth $t_{1,opt}$ in function of the diameter d, the in-plane angle α and the internal scanner set-up gives Eq. 4.

$$t_{opt} = t_{1,opt} = t_{2,opt} = \frac{c_{opt}}{\tan\alpha} = \frac{d \cdot \sin\frac{150°}{2}}{\tan\alpha} \qquad (4)$$

Figure 8 now shows the different theoretical and experimental scanning depths. The graph displays the curve for the maximum laser depth $t_{1,max}$ (Fig. 7a), the theoretical maximum measuring depth t_{opt} (Fig. 7c) and the experimental maximum measuring depth for the 30 degree in-plane angle in function of the diameter of the cylindrical cavity. Since the opening angle γ is limited, there is only a theoretical depth loss of 3.4%. The experimentally determined maximum depth deviates from this value mainly for the smaller and larger holes, with respect to the FOV of the scanner. The 1mm and 2mm holes have a too limited amount of data points to do a correct fitting. For the larger holes fewer laser light of the scanner will be reflected back diffusely onto the receiving sensor in comparison with the direct reflections on the bottom of the cavity. The main reason for the higher direct reflection on the bottom is the limited drilling aspect ratio of the larger holes. This results in a decrease of experimental measuring depth.

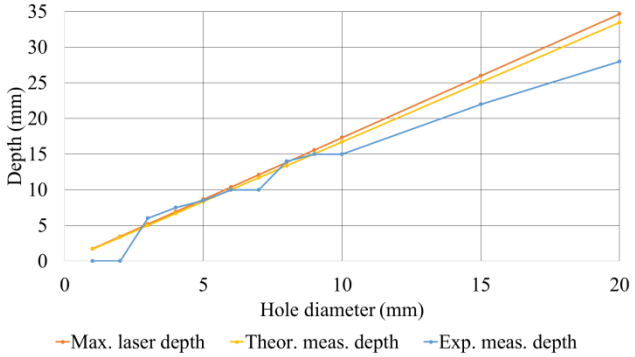

Fig. 8: Measurement depth in function of the diameter.

3.3.2 Accuracy in function of measuring depth

In section 3.2.2 it was already shown that the trends for the tactile and optical measurement resemble each other (Fig. 6). Also the order of magnitude of this deviation is similar for each pair of measurements, being 20 to -20µm for the x error and 10 to -10µm for the y error, for a depth range of 0mm to 18mm. The diameter measurements show a declining offset from the top of the hole to the deepest measurement position. The offset starts at around 15µm and can be addressed to the structural differences between the tactile and the optical measurement technique. The probe compensation which has to be taken into account for tactile measurements can be excluded for the optical method, because the coordinates are determined on the surface itself. For the optical technique surface quality and the CMOS sensor calibration are at play.

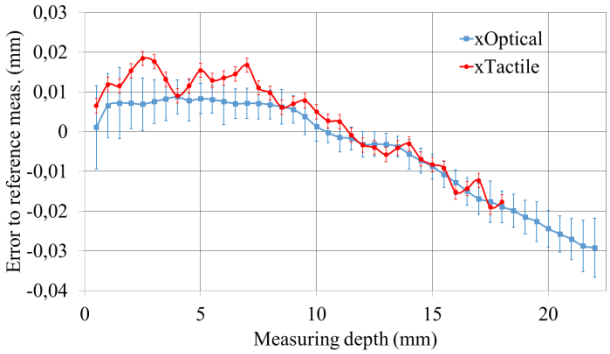

Fig. 9: Error value for the x position for the optical and tactile measurement in function of the measurement depth.

Figure 9 focusses on the comparison for the x position. The 6σ standard deviation estimator for the 5 measurements is superimposed on the graph for the optical measurement as an error bar. The average 6σ for the optical measurement amounts to 9µm on average and peaks to 14µm. The region close to the top plane is not taken into account. The rather high standard deviation can be explained by the fact only a limited number of measurements were done, which restricts the estimation capabilities for the standard deviation. In the case study the standard deviation is computed to a more accurate extent (section 4). Five extra measurements brought the standard deviation estimator to 7.5µm on average and a peak to 9.5µm. This proves the capability to be close to the stated accuracy of 9µm (LC60Dx).

For the tactile measurement the given MPE_P value of the machine (Eq. 1) was used with the tactile TP200 probe as sensor. This resulted in a total MPE_P of 1.8µm (position is not length dependent).

The trends are much alike as well as the error itself. The downward trend can be explained by the slight non orthogonal direction of the cylindrical hole. The nominal value to determine the error is, as explained earlier, the tactile reference measurement of the full cylinder. Since only small parts of the cylinder are assessed in the results shown above, both the optical and the tactile results show similar trends. Another remark is the more up-and-down tactile outcome. The searching zone for the fitting (2mm) is

somewhat wider than the measuring region for the tactile measurement (0.5mm), which means a more average result is acquired for the former of the two. This can also explain why a couple of the error bars do not find any overlapping zone.

Lastly, conclusions can be made on the presence of a preferable region to do measurements within a non-conical cavity. In nearly all measurements (x and y position and diameter measurands) the standard deviation of the five consecutive appraisals displays a bathtub tendency with a large zone optimum. The first and last measurements show higher standard deviation, respectively because of noise of the top plane and less accurate reflection points at the lowest region. In terms of accuracy most often an optimum is found around half way the maximum measurement depth. An example of this standard deviation trend and accuracy optimum is shown in Fig. 9. In that case the optimum can be found at around 10mm to 15mm depth.

4. CASE STUDY

4.1 Case study description

The case study involves the workpieces shown in Fig. 3b. The study objects have several cylindrical cavities of which the position and/or the diameter are assigned with tolerances on the technical drawing. A CAD-model was at hand, which made the programming load lighter. Within the case study the conclusions of section 3 are tested on an industrial part and the repeatability is evaluated. Based on the results of the diameter 8mm holes of the aspect ratio test the cavities in this case study (diameter 8.5mm) are measured at a depth of around 7.5mm with four sensor orientations all using an in-plane angle of 30 degrees. The comparison shown in section 4.3 is made with respect to another measurement, following basic guidelines for the scanner, using only two sensor orientations and a cylinder fitting close to the top surface. All other measurement settings are kept constant.

The repeatability study is using a basic set of 9 measurements for each separate feature. 12 features (6 for both the shiny and the matt part) are measured, which totals to 108 measurements for every technique used. Each three consecutive scans, the object is moved to another location on the CMM to also bring into play the inaccuracy of the measuring machine. A statistical analysis based on the standard deviation is used to determine a measure for the repeatability. The accuracy is estimated by comparing the average values of the 9 optical measurements with the 9 tactile measurements for each feature. The comparison of the two optical measurement approaches uses the same amount of optical measurements. The tactile section remains the same for both.

4.2 Results

Table 1 presents the measurement error for a sample of the optical measurements in contrast to the tactile reference for the case study object using the optimal measurement approach. Only a small selection of the x position measurements (3 out of 6 diameter 8.5mm holes for the shiny case study object) is shown to keep an overview. The full expanded table also includes the results for the matt case study object. Similar tables are constructed for the diameter and the y position. For the measurements following the supplied basic guidelines the same procedure is executed to make a comparison.

Table 1: Sample of case study results: measurement error for x position (in mm) according to the approach of section 3.

	Shiny object		
	Feat. 1	Feat. 2	Feat. 3
1	0,0037	-0,0162	-0,007
2	0,0029	-0,0196	-0,0049
3	0,0045	-0,0223	-0,0054
4	0,0011	-0,0222	-0,0048
5	0,0021	-0,0231	-0,0068
6	0,0007	-0,0221	-0,0074
7	0,0011	-0,0226	-0,0037
8	0,0013	-0,0232	-0,0047
9	0,0022	-0,0204	-0,0033

4.3 Discussion

4.3.1 Repeatability

Starting from the data (of which a sample was shown in Table 1) an elaborate repeatability and accuracy study is conducted for both optical measurement methods. The repeatability is determined for each feature (9 measurements, 8 degrees of freedom) and is also pooled for all assessed features (108 measurements, 96 degrees of freedom). The pooled standard deviations are depicted in Fig. 10 with the blue colour bars. Note that the pooling of the data takes place covering both case study workpieces. This is done to include surface finish in the pooled value. The separated pool values for the matt workpiece and the shiny workpiece (54 measurements each, 48 degrees of freedom) are also included in Fig. 10 to indicate the influence of the surface finish.

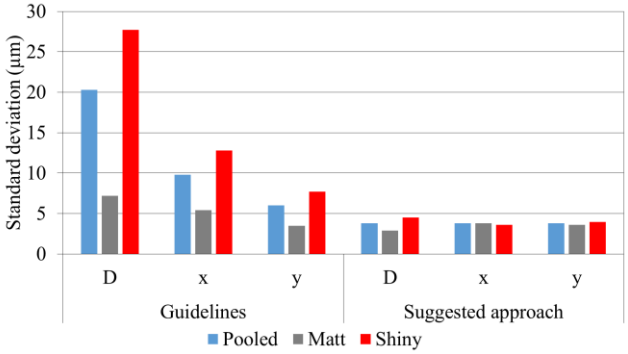

Fig. 10: Comparison of pooled and separated (according to surface finish) standard deviations for the two measurement methods.

Two main conclusions can be drawn from the bar chart (Fig. 10). Firstly, the suggested approach, determined in section 3, shows a better standard deviation for all but one measurand and is therefore more repeatable. The use of more sensor orientations combined with the selection of the cylinder subsection results in more stable measurements. The former assures a more spread point cloud over the feature, where some mantle sections are not scanned when using only two sensor orientations. The latter ensures the influence of the top plane and the bottom section to be ruled

out. Since the point extraction for the cylinder measurement is executed further below the top plane, no noise points can incorrectly be added to the cylinder measurement. Secondly, the separated values for the two surface finishes are a lot more similar for the suggested approach. Seemingly, the aforementioned reasons apply more on high surface finish parts. The scan patches resulting from a scan on a reflective part are smaller and hence less of the cylinder mantle is covered by the measurement data. In that case spreading the data points more equally becomes even more important for the feature extraction.

4.3.2 Accuracy

A second parameter to be assessed is the resulting accuracy for the method derived in this paper. Figure 11 shows the obtained average measurement error values with respect to the tactile reference measurement for a randomly picked feature (the third cavity of the matt case study object). The outcome for both methods shows the same order of magnitude for the error values. The differences obtained in this study varies from around 3µm on the average of 9 measurements up to 10µm. The latter was found for the shiny case study object, which has a higher standard deviation and can therefore alter to a larger extent for the approach based on the general guidelines for the scanning sensor.

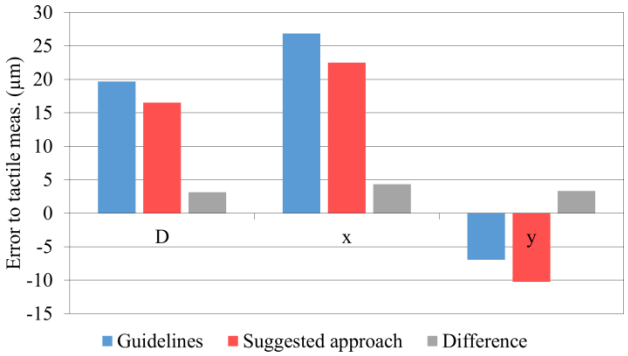

Fig. 11: Comparison of the measurement error to the tactile measurement of the two measurement methods for a feature of the matt case study object.

5. CONCLUSIONS

This paper provides an in depth study on the aspect ratio obtainable with an optical sensor, namely a laser scanner. The maximum depth for the full inspection of a cylindrical hole follows the theoretical curve with expected divergences for the smaller holes and the larger holes. The latter can be addressed to the phosphorescent surface finish added to the fact the aspect ratio of the hole itself is not tremendously high, creating a direct reflection chain that overtakes the diffuse reflection. In function of the measuring depth, the accuracy and repeatability of the measurement of a section of the hole both have an optimum in the middle of the accessible region. Aberrations from these values are caused by noise of adjacent features at the top of the cylindrical cavities and a lack of accurate measurement points in the bottom section.

The case study presents interesting results with respect to the measurement methods used. The newly determined approach shows important differences to the measurements according to the basic guidelines of the sensor. Through using the suggested method constructed during this study, the standard deviation of the measurement and therefore the repeatability improves. The measurement error to the tactile reference measurement remains within the same order of magnitude. The differences for the average measurement values recorded are limited to 3µm up to 10µm.

ACKNOWLEDGEMENTS

The research received funding from IWT through the Tetra project *Multi-sensor coördinaten meettechniek voor snel en accuraat opmeten van complexe producten (MuSeS - 12017)*.

REFERENCES

[1] H. Zhao, J.-P. Kruth, B. Boeckmans, N. Van Gestel, P. Bleys, “Automated dimensional inspection planning using the combination of laser scanner and tactile probe”, *Measurement*, vol.45(5), pp.1057-1066, 2012.

[2] N. Van Gestel, S. Cuypers, P. Bleys, J.-P. Kruth, “A performance evaluation test for laser line scanners on CMMs”, *Optics and Lasers in Engineering*, vol.47, pp.336-342, 2009.

[3] A. Contri, P. Bourdet, C. Lartigue, “Quality of 3D digitized points obtained with non-contact optical sensors”, *CIRP Annals – Manufacturing Technology*, vol.51(1), pp.443-446, 2002.

[4] C. Lartigue, A. Contri and P. Bourdet, “Digitised point quality in relation with point exploitation”, *Measurement*, Vol.6, pp.193-203, 2002.

[5] H. Feng, Y. Liu, F. Xi, “Analysis of digitizing errors of a laser scanning system”, *Precision Engineering*, Vol.25, pp.185-191, 2001.

[6] B. Igor, N. Van Gestel, J.-P. Kruth, P. Bleys, J. Hodolič, “Accuracy improvement of laser line scanning for feature measurements on CMM”, *Optics and Lasers in Engineering*, vol.45(11), pp.1274-1211, 2011.

[7] ISO 14253-1:1998. GPS – Inspection by measurement of workpieces and measuring equipment – Part 1: Decision rules for proving conformance or non-conformance with specifications.

[8] ISO 14253-2:2011. GPS – Inspection by measurement of workpieces and measuring equipment – Part 2: Guide to the estimation of uncertainty in GPS measurement, in calibration of measuring equipment and in product verification.

[9] ISO, GUM, JCGM 100:2008: Evaluation of measurement data – Guide to the espression of uncertainty in measurement.

[10] ISO 10360-8.2:2012. Geometrical Product Specifications (GPS) – Acceptance and reverification test for coordinate measuring machines (CMM) – Part 8: CMMs with optical distance sensors.

[11] A. Bernard, M. Véron, “Analysis and Validation of 3D Laser Sensor Scanning Process”, *CIRP Annals – Manufacturing Technology*, vol.48 (1), pp.111-114, 1999.

[12] B. Boeckmans, F. Welkenhuyzen, J.-P. Kruth, “Accuracy verification of a laser line scanner probe”, *Laser Metrology and Machine Performance X*, pp. 279-288, 2013.

[13] ISO 10360-1:2000. Geometrical Product Specifications (GPS) – Acceptance and reverification tests for coordinate measuring machines (CMM) – Part 1: Vocabulary.